

spacecraft, which represents the total magnetic flux transported from the dayside to the nightside magnetosphere by all processes, including viscous interaction¹⁴ and reconnection. For the solar wind conditions at hand (from Wind spacecraft: $V_{\text{SW}} = 550 \text{ km s}^{-1}$ and $B_{\text{SW}} = 7 \text{ nT}$, due south) the polar cap potential can be calculated¹⁵, from a large assembly of low-altitude satellite data, to be about 105 kV. This analysis indicates that, as has been hinted by indirect evidence^{16,17} but never confirmed by *in situ* measurements, reconnection is indeed the dominant process of solar wind entry when the solar wind magnetic field is persistently southward, with other processes having a minor role at most.

The reconnection electric field together with the length of the reconnection line determine what fraction of the solar wind particle flux and energy impinging on the magnetopause actually enters the magnetosphere. The presence of a 0.4 mV m^{-1} electric field across a dawn-to-dusk reconnection line indicates about 10% entry rate¹³. This translates to $\sim 10^{28}$ particles per second crossing the magnetopause from a flux of $\sim 10^{29}$ per second (based on solar wind density of 4 cm^{-3} and speed of 550 km s^{-1}) impinging on a magnetopause cross-section of $40 R_E$ in diameter. The corresponding total energy transfer into the magnetosphere is $2.5 \times 10^{12} \text{ W}$.

The observations presented here were made under a purely southward solar wind magnetic field geometry where most large-scale models of magnetopause reconnection^{1,8–11} predict an equatorial reconnection line, as observed. For other field orientations, the location and extent of the reconnection region are at present not known. To evaluate which model (for example, ‘component reconnection’^{8,9} versus ‘anti-parallel reconnection’¹⁰) best predicts the global reconnection configuration requires the identification of the reconnection sites for a variety of field orientations, a task that will be performed by the forthcoming four-spacecraft Cluster II mission. □

Received 21 October 1999; accepted 6 March 2000.

1. Dungey, J. W. Interplanetary magnetic field and the auroral zones. *Phys. Rev. Lett.* **6**, 47–48 (1961).
2. Cowley, S. W. H. in *Magnetic Reconnection in Space and Laboratory Plasmas* (ed. Hones, E. W.) 375–378 (Geophysics Monograph 30, American Geophysical Union, Washington, DC, 1984).
3. Nagai, T. *et al.* Structure and dynamics of magnetic reconnection for substorm onsets with Geotail observations. *J. Geophys. Res.* **103**, 4419–4440 (1998).
4. Akasofu, S.-I. Energy coupling between the solar wind and the magnetosphere. *Space Sci. Rev.* **28**, 121–190 (1981).
5. Paschmann, G. *et al.* Plasma acceleration at the earth’s magnetopause: Evidence for reconnection. *Nature* **282**, 243–246 (1979).
6. Sonnerup, B. U. Ö. Evidence for reconnection at the earth’s magnetopause. *J. Geophys. Res.* **86**, 10049–10067 (1981).
7. Gosling, J. T. *et al.* Accelerated plasma flows at the near-tail magnetopause. *J. Geophys. Res.* **91**, 3029–3041 (1986).
8. Gonzales, W. D. & Mozer, F. S. A quantitative model for the potential resulting from reconnection with an arbitrary interplanetary magnetic field. *J. Geophys. Res.* **79**, 4186–4194 (1974).
9. Sonnerup, B. U. Ö. Magnetopause reconnection rate. *J. Geophys. Res.* **79**, 1546–1549 (1974).
10. Crooker, N. U. Dayside merging and cusp geometry. *J. Geophys. Res.* **83**, 951–959 (1979).
11. Berchem, J. in *Physics of the Magnetopause* (eds Song, P., Sonnerup, B. U. Ö. & Thomsen, M. F.) 205–214 (Geophysics Monograph 90, American Geophysical Union, Washington, DC, 1995).
12. Paschmann, G. *et al.* The magnetopause for large magnetic shear: AMPTE/IRM observations. *J. Geophys. Res.* **91**, 11099–11115 (1986).
13. Lindqvist, P.-A. & Mozer, F. S. The average tangential electric field at the noon magnetopause. *J. Geophys. Res.* **95**, 17137–17144 (1990).
14. Axford, W. I. & Hines, C. O. A unifying theory of high-latitude geophysical phenomena and geomagnetic storms. *Can. J. Phys.* **39**, 1433–1464 (1961).
15. Burke, W. J., Weimer, D. R. & Maynard, N. C. Geoeffective interplanetary scale sizes derived from regression analysis of polar cap potentials. *J. Geophys. Res.* **104**, 9989–9994 (1999).
16. Fairfield, D. H. & Cahil, L. J. Jr Transition region magnetic field and polar magnetic disturbances. *J. Geophys. Res.* **71**, 155–170 (1966).
17. Cowley, S. W. H. in *Achievements of the International Magnetospheric Study (IMS)* 483–494 (SP-217, ESA, Paris, 1984).

Acknowledgements

We thank R. Lepping and R. Lin for making the Wind spacecraft data available, and A. Raj, H. Kucharek, D. Patel and P. Schroeder for their help in the processing of Equator-S plasma data. We also thank S. Krucker for comments on the manuscript.

Correspondence and requests for materials should be addressed to T.P. (e-mail: phan@ssl.berkeley.edu).

Statistical signatures of photon localization

A. A. Chabanov*, M. Stoytchev*† & A. Z. Genack*

*Physics Department, Queens College, The City University of New York, Flushing, New York 11367, USA

†Present address: Bell Labs, Lucent Technologies, Murray Hill, New Jersey 07974-0636, USA

The realization that electron localization in disordered systems¹ (Anderson localization) is ultimately a wave phenomenon^{2,3} has led to the suggestion that photons could be similarly localized by disorder³. This conjecture attracted wide interest because the differences between photons and electrons—in their interactions, spin statistics, and methods of injection and detection—may open a new realm of optical and microwave phenomena, and allow a detailed study of the Anderson localization transition undisturbed by the Coulomb interaction. To date, claims of three-dimensional photon localization have been based on observations of the exponential decay of the electromagnetic wave^{4–8} as it propagates through the disordered medium. But these reports have come under close scrutiny because of the possibility that the decay observed may be due to residual absorption^{9–11}, and because absorption itself may suppress localization³. Here we show that the extent of photon localization can be determined by a different approach—measurement of the relative size of fluctuations of certain transmission quantities. The variance of relative fluctuations accurately reflects the extent of localization, even in the presence of absorption. Using this approach, we demonstrate photon localization in both weakly and strongly scattering quasi-one-dimensional dielectric samples and in periodic metallic wire meshes containing metallic scatterers, while ruling it out in three-dimensional mixtures of aluminium spheres.

In the absence of inelastic and phase-breaking processes, the ensemble average of the dimensionless conductance ($\langle g \rangle \equiv \langle G \rangle / (e^2/h)$) is the universal scaling parameter¹² of the electron localization transition¹. Here $\langle \dots \rangle$ represents the average over an ensemble of random sample configurations, G is the electronic conductance, e is the electron charge, and h is Planck’s constant. The dimensionless conductance g can be defined for classical waves as the transmittance, that is, the sum over transmission coefficients connecting all

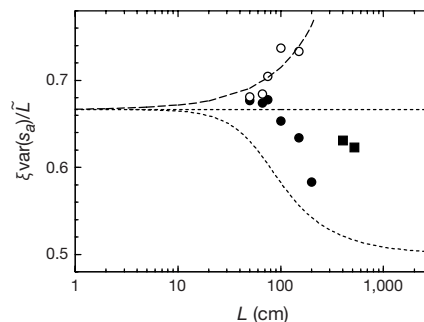


Figure 1 Influence of absorption and localization, separately and together, on $\text{var}(s_a)$ in random polystyrene samples. A semi-logarithmic plot of $\xi \text{var}(s_a)/L$ is presented to illustrate the measured scaling of $\text{var}(s_a)$ over a large range of L , as well as various theoretical predictions. The upper and lower short-dashed lines represent the two limits of diffusion theory: $L \ll \xi$, L_a and $L_a \ll L \ll \xi$, respectively. The filled circles are obtained from measurements of total transmission, while the filled squares are obtained from measurements of intensity. The open circles are the results of an analysis that eliminates the effect of absorption, as explained in the text. The upper, long-dashed curve is a fit of these results to an expression incorporating the first-order localization correction to diffusion theory.

input modes a and output modes b , $g \equiv \Sigma_{ab} T_{ab}$ (ref. 13). In the absence of absorption, $\langle g \rangle$ not only determines the scaling of transmission quantities, such as T_{ab} and $T_a = \Sigma_b T_{ab}$ that we will refer to as the intensity and total transmission, respectively, but it also determines their full distribution^{14–16}. In electronically conducting samples or in white paints, $\langle g \rangle \gg 1$ and Ohm's law holds, $\langle g \rangle = Nl/L$, where N is the number of transverse modes at a given frequency, l is the transport mean free path, and L is the sample length. But beyond the localization threshold, at $\langle g \rangle \approx 1$ (refs 12, 17), the wavefunction or classical field is exponentially small at the boundary and $\langle g \rangle$ falls exponentially with L . Localization can be achieved in a strongly scattering three-dimensional sample with a sufficiently small value of l (ref. 2), or even in weakly scattering samples in a quasi-one-dimensional geometry of fixed N , once L becomes greater than the localization length, $\xi = Nl$ (ref. 17). The latter corresponds to a wire in electronics or to a waveguide for microwave radiation.

In the presence of absorption, however, $\langle g \rangle$ cannot serve as a universal localization parameter because both the small value of $\langle g \rangle$ and its exponential scaling may simply reflect the effect of absorption. In this case, the decrease in $\langle g \rangle$ would represent a weakening rather than a strengthening of localization. Moreover, the distributions of the intensity and of the total transmission are affected by absorption and cannot be simply related to $\langle g \rangle$. Furthermore, it has been argued¹⁸ that $\langle g \rangle$ is not a natural scaling parameter because fluctuations in conductance are so large for localized waves that only the full conductance distribution or a parameter reflecting this

distribution properly expresses the nature of transport. We find for microwave radiation that for $L \leq \xi$ the full distribution of the intensity and total transmission normalized to their ensemble averages, $s_{ab} = T_{ab}/\langle T_{ab} \rangle$ and $s_a = T_a/\langle T_a \rangle$, respectively, can be well expressed in terms of a single parameter, the variance of the normalized total transmission, $\text{var}(s_a)$, even in strongly absorbing samples^{19,20}. This suggests that $\text{var}(s_a)$ might serve as a localization parameter. Large values of $\text{var}(s_a)$ would be expected for sharp spectra with widely spaced peaks that occur for localized waves. Further, because $\text{var}(s_a) = 2/3\langle g \rangle$ for $L \ll \xi, L_a$, where L_a is the absorption length, and because the localization threshold occurs at $\langle g \rangle \approx 1$ in the absence of absorption, we make the conjecture that localization is achieved when $\text{var}(s_a) \geq 2/3$. This localization condition may be expressed in a familiar form by defining a new localization parameter $g' \equiv 2/3\text{var}(s_a)$, which reduces to $\langle g \rangle$ in the absence of absorption in the limit $\text{var}(s_a) \ll 1$. Localization is then achieved for $g' \leq 1$ whether absorption is present or not.

In previous measurements of total transmission, $\text{var}(s_a)$ was found to increase sublinearly with length for diffusive waves in strongly absorbing quasi-one-dimensional dielectric samples¹⁹. This raised the possibility that the value of $\text{var}(s_a)$ might saturate with length, and that absorption might introduce a cut-off length for the renormalization of transport. Here we show that, though the presence of absorption leads to a decrease in $\text{var}(s_a)$, this appropriately reflects a lessening of localization effects. The threshold for localization occurs at $g' \approx 1$, and for smaller values, g' falls exponentially with length.

We now consider wave transport statistics in a quasi-one-dimensional geometry. Because L is much greater than the transverse dimensions of a quasi-one-dimensional sample, energy injected at any point of the input is equally likely to emerge at any point of the output, and modes are completely mixed by the medium. As a result, statistical measurements at any point on the output surface of the sample or in any of its transmission modes yield identical results, and depend upon the sample geometry only through the ratio $\xi/L = \langle g \rangle$. For $N \gg 1$, scattering is locally three-dimensional and wave transport may be given a universal description.

We will first consider the scaling of $\text{var}(s_a)$ and its connection to localization in strongly absorbing weakly scattering dielectric samples contained in a copper tube. The role of absorption will be investigated by comparing these measurements to an analysis of the data that statistically eliminates the influence of absorption. Measurements are carried out in samples of loosely packed, 1.27-cm-diameter polystyrene spheres with a filling fraction of 0.52 within the frequency range 16.8–17.8 GHz. In these samples, $l \approx 5$ cm (ref. 21), giving $\xi \approx 5$ m for a tube diameter of 5 cm. The exponential attenuation length due to absorption is $L_a = 0.34 \pm 0.02$ m (ref. 19), and the diffusion extrapolation length, which gives an effective sample length for the statistics of transmission²², $\tilde{L} = L + 2z_b$, is

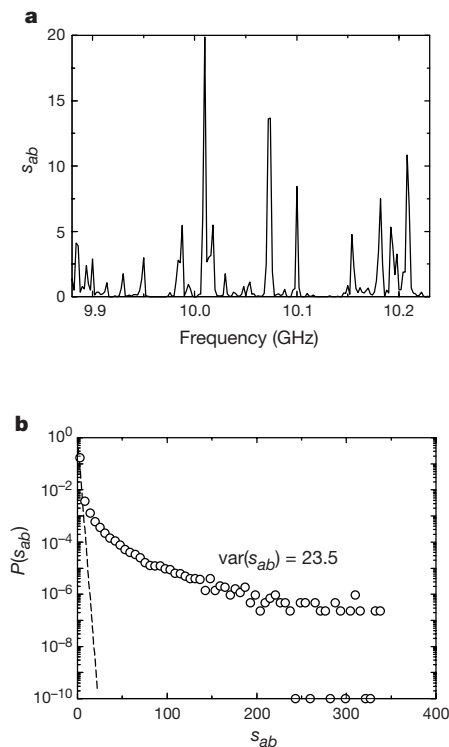


Figure 2 Statistics of intensity in quasi-one-dimensional alumina samples. Alumina spheres (diameter $d_a = 0.95$ cm, dielectric constant $\epsilon_a = 9.8$) embedded in Styrofoam shells ($d_s = 1.9$ cm, $\epsilon_s = 1.05$) at an alumina volume fraction of 0.068 are contained in an 80-cm-long, 7.3-cm-diameter copper tube. A typical spectrum of the normalized intensity s_{ab} (panel **a**) and the distribution $P(s_{ab})$ (panel **b**) near the first Mie resonance of the alumina spheres are presented. The sharp and narrow line spectra and giant fluctuations shown have been predicted for localized waves, and are unlike corresponding spectra and distributions in diffusive samples²³. The distribution $P(s_{ab})$ plotted on a semi-logarithmic scale is computed in an ensemble of 5,000 sample configurations within the frequency range 9.88–10.24 GHz, in which statistical parameters do not change substantially. The broken line shows the Rayleigh distribution.

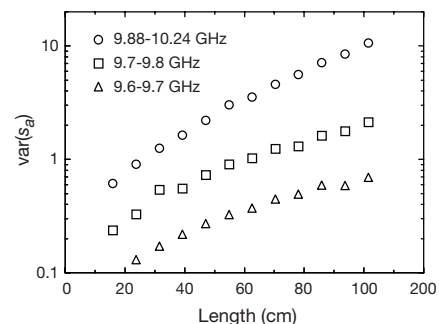


Figure 3 Scaling of $\text{var}(s_a)$ in alumina samples. The values of $\text{var}(s_a)$ averaged over the indicated frequency intervals are obtained using equation (1). Above a value of the order of unity, $\text{var}(s_a)$ increases exponentially. In the interval 9.88–10.24 GHz, $\text{var}(s_a) \approx \exp(L/L_{\text{exp}})$, with $L_{\text{exp}} \approx 42$ cm.

$z_b \approx 6$ cm (ref. 21). For $L \ll \xi$, L_a , diffusion theory gives $\text{var}(s_a) = 2\bar{L}/3\xi$ (refs 14, 15). This result is shown as the horizontal short-dashed line in Fig. 1. Measurements of fluctuations in the spectrum of total transmission in ensembles of polystyrene samples give the results shown as the filled circles in Fig. 1. These results indicate that $\text{var}(s_a)$ increases sublinearly with length up to $L = 2$ m, which was the largest length at which accurate measurements of the total transmission could be made.

Values of $\text{var}(s_a)$ can also be obtained from measurement of the intensity T_{ab} . Our measurements of intensity and total transmission confirm the predicted relation between the moments of the normalized intensity and total transmission¹⁵, $\langle s_{ab}^n \rangle = n! \langle s_a^n \rangle$. This allows us to relate the variance of the normalized transmission to the variance of the normalized intensity, which is more readily measured in microwave experiments

$$2\text{var}(s_a) = \text{var}(s_{ab}) - 1 \quad (1)$$

Using this relation, we are able to extend our study of statistics in random waveguides to greater lengths. We measured transmitted field spectra in an ensemble of 2,000 polystyrene samples with the use of a Hewlett-Packard 8772C network analyser. The calculated intensity spectra yield $\text{var}(s_{ab})$, which gives the corresponding values of $\text{var}(s_a)$ using equation (1). Values of $\text{var}(s_a)$ obtained in this way for $L \leq 2$ m agree to within 3% with those shown as the filled circles in Fig. 1. The results for $L > 2$ m are shown in the figure as the filled squares. They indicate a more rapid, superlinear increase in $\text{var}(s_a)$ relative to the data for $L \leq 2$ m.

In these measurements, the effect of developing localization and absorption are intertwined. In order to obtain the values of $\text{var}(s_a)$ that would be measured in the absence of absorption, the field spectra are Fourier-transformed to give the response to a narrow gaussian pulse in the time domain. To compensate for losses due to absorption, the time-dependent field is multiplied by $\exp(t/2\tau_a)$, where t is the time delay from the incident pulse and $1/\tau_a$ is the absorption rate determined from measurements of the field correlation function with frequency shift²³. This new field is transformed back to the frequency domain. Intensity spectra and the distribution and variance of intensity are then computed. The intensity distributions are in excellent agreement with calculations for diffusive waves^{14,15}, which are described in terms of a single parameter (g). The values of $\text{var}(s_a)$ found in this way are shown as the open circles in

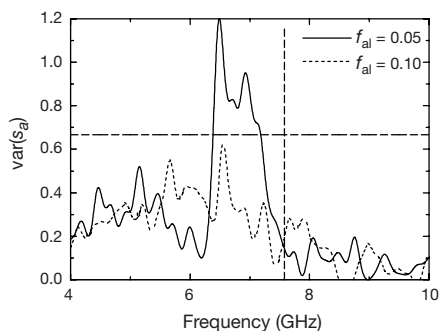


Figure 4 $\text{var}(s_a)$ versus frequency in a wire-mesh photonic crystal containing metal scatterers. The photonic crystal is a simple cubic lattice made up of copper wires, with a lattice constant of 1 cm. The lattice has 8 unit cells along each side. It is enclosed in a section of a square waveguide and filled with mixtures of 0.47-cm-diameter aluminium and Teflon spheres, the latter used to dilute the aluminium scatterers. Measurements of intensity are carried out in 200 sample configurations, and $\text{var}(s_a)$ is obtained using equation (1). The broken vertical line indicates the position of the band edge in a periodic structure filled only with Teflon spheres. At an aluminium sphere volume fraction (f_{al}) of 0.05, $\text{var}(s_a)$ is markedly higher near the edge, rising above the localization threshold of 2/3 shown as the broken horizontal line.

Fig. 1. A fit of the leading order localization correction¹⁴, $\text{var}(s_a) = 2\bar{L}/3\xi + 4\bar{L}^2/15\xi^2$, to the data gives the upper long-dashed curve in Fig. 1 with $\xi = 5.51 \pm 0.18$ m and $z_b = 5.25 \pm 0.31$ cm. The results are consistent with independent determination of these parameters²¹. The difference between the open and filled circles represents the amount by which $\text{var}(s_a)$ is reduced, and hence represents the extent to which localization is suppressed by absorption.

For diffusing waves, $\text{var}(s_a)$ is predicted to fall from $2\bar{L}/3\xi$ for $L \ll L_a$, to $\bar{L}/2\xi$ for $L \gg L_a$ (refs 24, 25), following the lower short-dashed curve in Fig. 1. Notwithstanding the initial drop of $\text{var}(s_a)$ from $2\bar{L}/3\xi$, our measurements rise above this curve as a result of enhanced intensity correlation, as $L \rightarrow \xi$. At $L = 5.2$ cm, $\text{var}(s_a) = 0.6$, which is close to the critical value of 2/3.

To study the statistics of s_a for localized waves, we examine fluctuations of intensity in strongly scattering quasi-one-dimensional samples of alumina (Al_2O_3) spheres. A typical spectrum of s_{ab} obtained near the first Mie resonance of the spheres is shown in Fig. 2a. The sharp peaks in s_{ab} result from resonant transmission through localized photonic states in the medium. The distribution function $P(s_{ab})$ calculated for an ensemble of 5,000 samples is shown in Fig. 2b and compared to the Rayleigh distribution. The measured distribution is remarkably broad, with $\text{var}(s_{a,b}) = 23.5$ and fluctuations greater than 300 times the average value. The scaling of $\text{var}(s_a)$ determined using equation (1) at a number of frequencies is shown in Fig. 3. We find $\text{var}(s_a)$ increases exponentially once it becomes of the order of unity, as expected for a localization parameter.

The availability of a measurable localization parameter makes it possible to determine the existence and the extent of localization in a variety of samples. This is illustrated in measurements of localization in periodic metallic wire meshes containing metallic scatterers. John has proposed that photon localization could be achieved by introducing disorder in a periodic structure possessing a photonic bandgap²⁶. Measurements of transmission in the wire-mesh photonic crystal show a low-frequency gap²⁷, which fills in as the scatterer density is increased²⁸. But such measurements leave open the question of whether the radiation is localized. To answer this question, we obtain $\text{var}(s_a)$ for two concentrations of aluminium spheres shown in Fig. 4. At a volume fraction of aluminium spheres of 0.05, a window of localization is found, in which $\text{var}(s_a) \geq 2/3$. At twice this aluminium fraction, the reduced values of $\text{var}(s_a)$ indicate that wave propagation is diffusive.

We have also used measurements of $\text{var}(s_a)$ to examine the claim that localization can be achieved in three-dimensional samples of metal spheres at various concentrations^{4,5,29,30}. We find that in samples of 0.47-cm-diameter aluminium spheres of length $L = 8.2$ cm and diameter $d = 7.5$ cm, with various volume fractions from 0.1 to 0.475, $\text{var}(s_a)$ never rises above the localization threshold of 2/3. A maximum value of 0.29 is reached at a concentration of 0.45. Thus three-dimensional localization is not achieved in these aluminium samples. These results demonstrate that $\text{var}(s_a)$ is a powerful guide in the search for and characterization of photon localization. □

Received 23 August; accepted 1 March 2000.

- Anderson, P. W. Absence of diffusion in certain random lattices. *Phys. Rev.* **109**, 1492–1505 (1958).
- Ioffe, A. F. & Regel, A. R. Non-crystalline, amorphous and liquid electronic semiconductors. *Prog. Semicond.* **4**, 237–291 (1960).
- John, S. Electromagnetic absorption in a disordered medium near a photon mobility edge. *Phys. Rev. Lett.* **53**, 2169–2172 (1984).
- Garcia, N. & Genack, A. Z. Anomalous photon diffusion at the threshold of the Anderson localization transition. *Phys. Rev. Lett.* **66**, 1850–1853 (1991).
- Genack, A. Z. & Garcia, N. Observations of the Anderson transition for electromagnetic radiation. *Phys. Rev. Lett.* **66**, 2064–2067 (1991).
- Wiersma, D. S., Bartolini, P., Lagendijk, A. & Righini, R. Localization of light in a disordered medium. *Nature* **390**, 671–673 (1997).
- Wiersma, D. S., Rivas, J. G., Bartolini, P., Lagendijk, A. & Righini, R. Localization or classical diffusion of light? (Reply) *Nature* **398**, 207 (1999).
- Vlasov, Ya. A., Kaliteevski, M. A. & Nikolaev, V. V. Different regimes of light localization in a disordered photonic crystal. *Phys. Rev. B* **60**, 1555–1562 (1999).

9. Scheffold, F., Lenke, R., Tweer, R. & Maret, G. Localization or classical diffusion of light? *Nature* **398**, 206–207 (1999).
10. Weaver, R. L. Anomalous diffusivity and localization of classical waves in disordered media: The effect of dissipation. *Phys. Rev. B* **47**, 1077–1080 (1993).
11. Yosefin, M. Localization in absorbing media. *Europhys. Lett.* **25**, 675–680 (1994).
12. Abrahams, E., Anderson P. W., Licciardello, D. C. & Ramakrishnan, T. V. Scaling theory of localization: absence of quantum diffusion in two dimensions. *Phys. Rev. Lett.* **42**, 673–676 (1979).
13. Landauer, R. Electrical resistance of disordered one-dimensional lattices. *Philos. Mag.* **21**, 863–867 (1970).
14. van Rossum, M. C. W. & Nieuwenhuizen, Th. M. Multiple scattering of classical waves: microscopy, mesoscopy, and diffusion. *Rev. Mod. Phys.* **71**, 313–372 (1999).
15. Kogan, E. & Kaveh, M. Random-matrix-theory approach to the intensity distributions of waves propagating in a random medium. *Phys. Rev. B* **52**, R3813–R3815 (1995).
16. van Langen, S. A., Brouwer, P. W. & Beenakker, C. W. J. Nonperturbative calculation of the probability distribution of plane-wave transmission through a disordered waveguide. *Phys. Rev. E* **53**, R1344–R1347 (1996).
17. Thouless, D. J. Maximum metallic resistance in thin wires. *Phys. Rev. Lett.* **39**, 1167–1169 (1977).
18. Shapiro, B. Scaling properties of probability distributions in disordered systems. *Philos. Mag.* **B 56**, 1031–1044 (1989).
19. Stoytchev, M. & Genack, A. Z. Measurement of the probability distribution of total transmission in random waveguides. *Phys. Rev. Lett.* **79**, 309–312 (1997).
20. Stoytchev, M. & Genack, A. Z. Observations of non-Rayleigh statistics in the approach to photon localization. *Opt. Lett.* **24**, 262–264 (1999).
21. Garcia, N., Genack, A. Z. & Lisyansky, A. A. Measurement of the transport mean free path of diffusing photons. *Phys. Rev. B* **46**, 14475–14479 (1992).
22. Lagendijk, A., Vreeker, R. & de Vries, P. Influence of internal reflection on diffusive transport in strongly scattering media. *Phys. Lett. A* **136**, 81–88 (1989).
23. Garcia, N. & Genack, A. Z. Crossover to strong intensity correlation for microwave radiation in random media. *Phys. Rev. Lett.* **63**, 1678–1681 (1989).
24. Garcia, N., Genack, A. Z., Pnini, R. & Shapiro, B. Intensity correlation in waveguides. *Phys. Lett. A* **176**, 458–461 (1993).
25. Brouwer, P. W. Transmission through a many-channel random waveguide with absorption. *Phys. Rev. B* **57**, 10526–10531 (1998).
26. John, S. Strong localization of photons in certain disordered dielectric superlattices. *Phys. Rev. Lett.* **58**, 2486–2489 (1987).
27. Sigalas, M. M., Chan, C. T., Ho, K. M. & Soukoulis, C. M. Metallic photonic band-gap materials. *Phys. Rev. B* **52**, 11744–11751 (1995).
28. Stoytchev, M. & Genack, A. Z. Microwave transmission through a periodic three-dimensional metal-wire network containing random scatterers. *Phys. Rev. B* **55**, R8617–R8621 (1997).
29. Arya, K., Su, Z. B. & Birman, J. L. Anderson localization of electromagnetic waves in a dielectric medium of randomly distributed metal particles. *Phys. Rev. Lett.* **57**, 2725–2728 (1986).
30. Condat, C. A. & Kirkpatrick, T. R. Observability of acoustical and optical localization. *Phys. Rev. Lett.* **58**, 226–229 (1987).

Acknowledgements

We thank P. W. Brouwer and E. Kogan for discussions. This work was supported by the NSF.

Correspondence and requests for materials should be addressed to A. A. C. (e-mail: achqc@qcuniv1.acc.qc.edu).

Spontaneous macroscopic magnetization at the superconducting transition temperature of $\text{YBa}_2\text{Cu}_3\text{O}_{7-\delta}$

R. Carmi, E. Polturak, G. Koren & A. Auerbach

Physics Department, Technion—Israel Institute of Technology, Haifa 32000, Israel

A noteworthy feature of the high-temperature superconductors is the unconventional symmetry of the superconducting order parameter. Several experiments^{1–3} have established that the order parameter has a four-fold $d_{x^2-y^2}$ symmetry under rotation of the lattice (the order parameter of conventional superconductors is, in contrast, isotropic). An intriguing and much debated possibility is that, in certain cases, an additional imaginary component might be present, having an isotropic s -wave^{4–6} or d_{xy} symmetry^{7–10}. A consequence of a complex order parameter of the form $d_{x^2-y^2} + id_{xy}$ is that it would break both reflection

(parity, P) symmetry and time-reversal (T) symmetry, a clear signature of which would be the spontaneous appearance of a macroscopic magnetization at the superconducting transition temperature. Broken T symmetry has been reported^{5,11}, but searches for the effects of combined P and T symmetry breaking have so far yielded null results^{12–15}. Here we report the observation of a weak ($\sim 10^{-5}$ gauss) magnetic field that appears spontaneously at the superconducting transition temperature of epitaxial thin films of $\text{YBa}_2\text{Cu}_3\text{O}_{7-\delta}$. The magnetic signal originates near the edges of the samples. One interpretation for this observation is that the order parameter carries an intrinsic angular momentum, related to the breaking of P and T symmetries, but other possibilities cannot yet be excluded.

Previous experimental searches of combined P and T violation set a limit of a few per cent on any symmetry-breaking component of the order parameter^{12–15}. If a spontaneous magnetic field below this limit were to exist, it may be easier to detect it by looking at the magnetic flux produced by the whole sample, instead of a small region. This is conditional upon such a field having the same orientation everywhere in the superconductor. To check this possibility, in our experiment we placed high-quality epitaxial, c -axis-oriented $\text{YBa}_2\text{Cu}_3\text{O}_{7-\delta}$ films on top of an input coil of a d.c. SQUID (superconducting quantum interference device) magnetometer operating at 77 K (see Fig. 1a). The magnetometer (M2700L, Conductus, Inc.) has a large, 8 mm \times 8 mm directly coupled single input loop. The magnetometer is operated in a flux locked loop, with either a.c. or d.c. bias.

Films of $\text{YBa}_2\text{Cu}_3\text{O}_{7-\delta}$ were prepared either by laser ablation deposition or d.c. sputtering on 1 cm \times 1 cm substrates, including (100)SrTiO₃, (100)MgO and (001)NdGaO₃. The range of thickness was between 30 nm and 300 nm, with the superconducting transition temperature, T_c , typically around 90 K. The films were measured as deposited, or after patterning into different structures

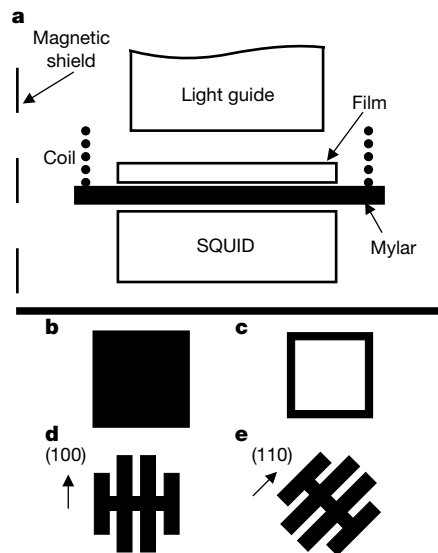


Figure 1 Schematic illustration of the experimental geometry and of the sample patterns. **a**, Cross-section of the experimental set-up. Light is introduced briefly through the light guide to heat the sample above T_c , and is turned off during the measurements. **b–e**, Film patterns used in this work. Magnetic shields reduce the residual field down to 10^{-4} G. Additional coils are used to further reduce this field, or to check for any field dependence. In order to avoid stray fields generated by currents used in resistive heating, the films are heated by a guided light beam; to eliminate any thermoelectric currents, the sample holder and all nearby components were made of non-magnetic plastic. Cooling of the samples is done using He exchange gas. The temperature of the films is measured *in situ* using the resistance of a carbon film painted onto the substrate. We verified that the small a.c. current used to measure the thermometer does not affect the results.